

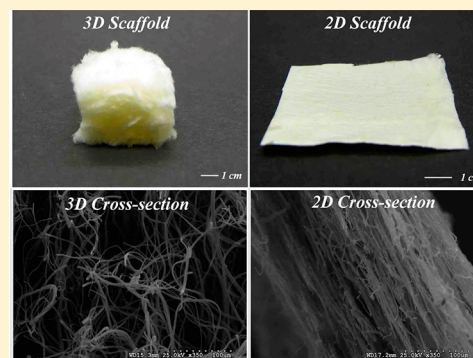
Novel 3D Electrospun Scaffolds with Fibers Oriented Randomly and Evenly in Three Dimensions to Closely Mimic the Unique Architectures of Extracellular Matrices in Soft Tissues: Fabrication and Mechanism Study

Shaobo Cai,[†] Helan Xu,[†] Qiuran Jiang,[†] and Yiqi Yang^{*,†,‡}

[†]Department of Textiles, Merchandising and Fashion Design, 234, HECO Building, University of Nebraska—Lincoln, Lincoln, Nebraska 68583-0802, United States

[‡]Department of Biological Systems Engineering, Nebraska Center for Materials and Nanoscience, 234, HECO Building, University of Nebraska—Lincoln, Lincoln, Nebraska 68583-0802, United States

ABSTRACT: In this work, novel electrospun scaffolds with fibers oriented randomly and evenly in three dimensions (3D) including in the thickness direction were developed based on the principle of electrostatic repulsion. This unique structure is different from most electrospun scaffolds with fibers oriented mainly in one direction. The structure of novel 3D scaffolds could more closely mimic the 3D randomly oriented fibrous architectures in many native extracellular matrices (ECMs). The cell culture results of this study indicated that, instead of becoming flattened cells when cultured in conventional electrospun scaffolds, the cells cultured on novel 3D scaffolds could develop into stereoscopic topographies, which highly simulated *in vivo* 3D cellular morphologies and are believed to be of vital importance for cells to function and differentiate appropriately. Also, due to the randomly oriented fibrous structure, improvement of nearly 5 times in cell proliferation could be observed when comparing our 3D scaffolds with 2D counterparts after 7 days of cell culture, while most currently reported 3D scaffolds only showed 1.5- to 2.5-fold improvement for the similar comparison. One mechanism of this fabrication process has also been proposed and showed that the rapid delivery of electrons on the fibers was the crucial factor for formation of 3D architectures.



1. INTRODUCTION

Ideal tissue engineering scaffolds should be capable of closely mimicking the topographies and spatial structures of native extracellular matrices (ECMs) to facilitate cells to grow and differentiate following the patterns similar to that found in native tissues and organs.^{1–3} Morphologies of ECMs vary according to functions of target tissues and cell types in the tissues.^{3–5} For example, in skin tissue, the top layer is formed by compact packing of epithelial cells on a two-dimensional (2D) fibrous ECM basement membrane. Three-dimensional spatial spreading of fibroblasts and immune cells occurs in the interior region of the skin tissue, and correspondingly the ECMs are constructed by stereoscopically and randomly oriented ultrafine protein fibers.^{6,7} Fibrous structures with 3D orientation and random distribution can also be found in native ECMs in breast,⁸ liver,⁹ bladder,¹⁰ lung,¹¹ and many other organs and tissues.¹² It has been reported that cells cultured on flat 2D substrates may differ considerably in morphology and differentiation pattern from those cultured in more physiological 3D environments.^{13,14} Therefore, it is reasonable to fabricate scaffolds with particular morphologies and structures according to categories and functions of original native tissues.^{15–18}

Due to its simplicity and high efficiency, electrospinning has been widely employed to fabricate tissue engineering scaffolds composed of nano- or submicrometer- fibers from numerous materials.^{19–24} However, conventional electrospun structures typically form 2D scaffolds with fibers aligned parallel to the collector and cells cultured on the conventional electrospun scaffolds could only develop into flat shapes. The functions and differentiation of many flattened cells could not resemble the native stereoscopic cells.²⁵ Furthermore, small pore sizes owing to the close arrangement of fibers restricted access of cells to interior of the conventional electrospun scaffolds. Thus, on conventional electrospun scaffolds, cells could mainly spread and distribute within a shallow depth beneath the surface.²⁶

To date, many 3D electrospinning techniques have been developed to fabricate electrospun scaffolds with larger pores and higher porosity to improve cell accessibility of the scaffolds; however, to the best of our knowledge, no studies have reported successful fabrication of scaffolds with three-dimensionally randomly oriented fibrous structures that could support

Received: November 6, 2012

Revised: January 19, 2013

Published: February 7, 2013

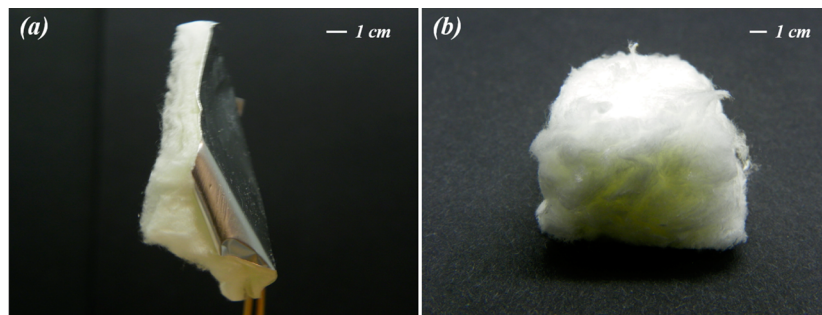


Figure 1. Digital photo of 3D zein electrospun scaffolds: (a) as-spun scaffold on aluminum foil; (b) scaffold ready for wash and use for cell culture.

cells to grow and spread in three dimensions as seen in native ECMs. Cells cultured on current 3D scaffolds still tended to have flattened morphologies, and thus differed structurally from stereoscopically developed cells in many native tissues. In addition, the parallel fibrous layer-by-layer structures led to difficulty in forming pores in thickness direction with sizes comparable to those in planar directions, and resultantly limited the improvement of scaffold porosity. The reason is that the basic principle of most current 3D electrospinning techniques, such as wet electrospinning,²⁷ electrospinning with integration of coarse fibers,²⁸ and electrospinning with porogens,²⁹ is physical blocking. Coagulation bath frameworks consisted of coarse fibers and porogenic agents, such as dry ice or sucrose, utilized in the above-mentioned techniques could physically increase distances between the electrospun fibers and lead to deeper penetration of cells into interior of scaffolds to some extent, but could not totally change the planar orientations of the electrospun fibers.

Recently, a few studies reported fabrication of 3D electrospun scaffolds based on the electrostatic repulsion between as-spun fibers;³⁰ however, despite the fluffy appearance of the scaffolds, it is found that these 3D scaffolds generated by electrostatic repulsion were still laminated with planar mats and parallel oriented fibers. In addition, the proposed mechanisms that a 3D scaffold was formed by the electrostatic repulsion between as-spun fibers failed to explain the formation process of randomly oriented fibrous structure. In this study, a novel 3D electrospinning scaffold was developed with ultrafine fibers oriented randomly and evenly in three dimensions which therefore could more effectively mimic the 3D fibrous structures in native ECMs and could support development of stereoscopic cells. A mechanism based on the highly increased surface conductivity of materials was proposed and validated.

Zein was used as a model material and 3D zein electrospun scaffolds were developed via the novel 3D electrospinning technique. Zein is a plant protein with satisfactory biocompatibility and low immunogenicity and has been electrospun into 2D scaffolds for tissue engineering.³¹

2. RESULTS AND DISCUSSION

2.1. Structural Characterization. As seen from the digital images in Figures 1 and 2a, 3D (Figures 1 and Figure 2a (left)) scaffold with porosity of 99.6% has remarkably higher fluffiness than 2D (Figure 2a (right)) scaffold with porosity of 79.4% of the same weight. In scanning electron microscopy (SEM) images of the 2D zein scaffold, the front views (Figure 2c and c') demonstrated that fibers packed closely, and in the side views (Figure 2e and e') tightly stacked sheets were observed. From both views, only a few pores larger than 10 μm could be

found. However, the fibers in 3D zein scaffold packed loosely, and multiple pores with sizes larger than 100 μm could be seen on the top surface (Figure 2d and d') and side (Figure 2f and f'). As reported, migration and penetration of cells into the interior of scaffolds necessitated introduction of pores larger than 100 μm into the structures.^{32,33} Thus, 3D scaffolds developed in this study would be preferred in cell culture due to the larger space available for cells to attach and infiltrate.

Furthermore, three-dimensionally randomly oriented fibers in all directions including the thickness direction rendered the 3D zein scaffold structurally more similar to that in the native ECMs. As seen from the SEM (Figure 2c–f) and confocal laser scanning microscopy (CLSM) images (Figure 2g–j), random arrangement and haphazard orientation of fibers could be observed in the 3D zein scaffold, while regularly piled fibrous mats in the 2D zein scaffold indicated few fibers oriented in the thickness direction. Therefore, compared to that on 2D scaffolds with highly stacked structures, cells cultured on 3D scaffolds would develop into more ellipsoidal and stereoscopic types.³⁴

To verify the potential of applying this novel 3D electrospinning method to materials other than proteins, polyethylene glycol (PEG) was 3D electrospun as well. The 3D and 2D PEG electrospun scaffolds are shown in Figure 2b left and right, respectively. The 3D PEG scaffold was also featured for the high pore content and loose structure as 3D zein scaffold, whereas the 2D PEG scaffold with tight structure, which resembled 2D zein scaffold.

2.2. Proposed Mechanism. 2.2.1. Theory of Mechanism.

Difference in 2D and 3D electrospinning structures was assumed to be induced by different transient electrical force when fibers hit collecting board. It is proposed that sufficiently high surface electrical conductivity or low electrical resistivity of polymer is the premise for formation of 3D scaffolds. In both conventional and 3D electrospinning, at the beginning, the liquid droplet acquired negative charges and then was elongated into fibers. As shown in Figure 3, both conventional (Figure 3a and c) and 3D (Figure 3b and d) electrospun fibers with large amount of surface negative charges flew toward the collecting board perpendicularly. For conventional electrospinning, few of electrons transferred to the collector at the moment the fiber ends hit the collector, owing to high surface resistivity of the fibers. The fibers with large amount of remaining electrons were strongly attracted by the positive collector. As a consequence, conventional 2D electrospun scaffolds with fibers oriented parallel to the collecting board were obtained.

Contrastively, for 3D electrospinning, low surface resistivity of fiber led to high transferability of charges from the fiber surface to the collector. When the fibers stroke the collector,

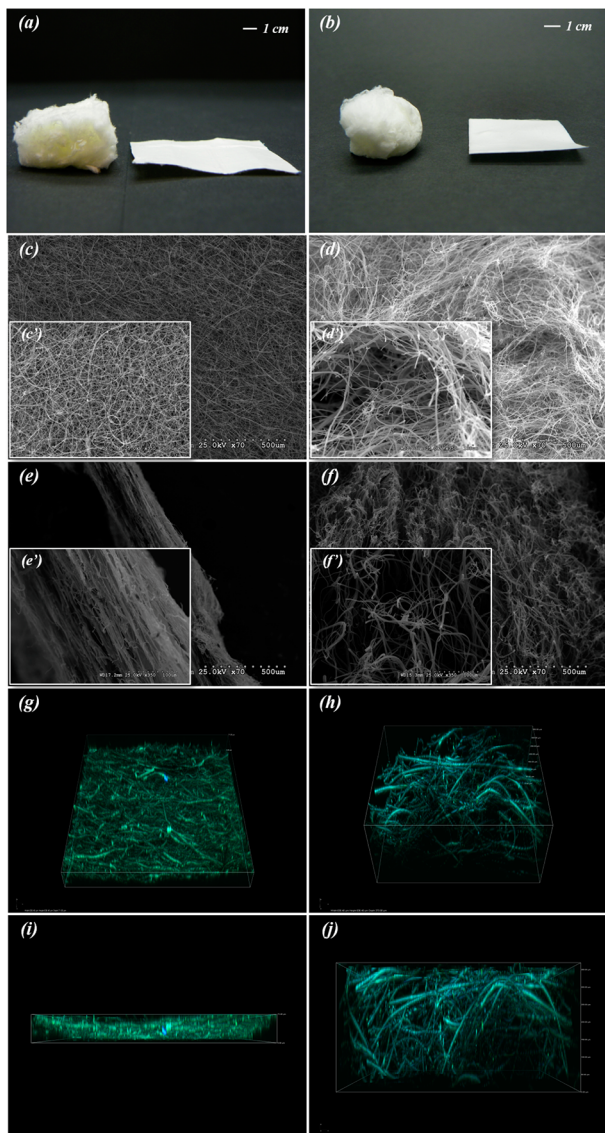


Figure 2. Morphological comparison between 2D and 3D electrospun zein and PEG scaffolds. (a) Digital photo of 3D (left) and 2D (right) zein electrospun scaffolds with the same weight. (b) Digital photo of 3D (left) and 2D (right) PEG electrospun scaffolds with the same weight. (c, c', d, d') SEM top view images at magnifications of 70 \times (c) and 350 \times (c') of 2D zein electrospun scaffold and 70 \times (d) and 350 \times (d') of 3D zein electrospun scaffold. (e, e', f, f') SEM side view images at magnifications of 70 \times (e) and 350 \times (e') of 2D zein electrospun scaffold and 70 \times (f) and 350 \times (f') of 3D zein electrospun scaffold. (g, h) CLSM 45° view images at magnification of 100 \times of 2D (g) and 3D (h) zein scaffolds. (i, j) CLSM side view image at magnification of 100 \times of 2D (i) and 3D (j) zein electrospun scaffolds.

surface static charge could transfer to the board in a much faster manner; thus, less electrons were left on the fibers, and decreased attraction between fibers and collector. In some cases, the near portions of the fibers could even carry positive charges and could be repulsed by the collector, while rear ends of the fibers were still attracted and moved toward the board. As a consequence, fibers were collected onto the board in multiple orientations and resulted in loose and fluffy 3D scaffolds.

2.2.2. Validation. A power function was used to simulate the relationship between the specific pore volume of electrospun

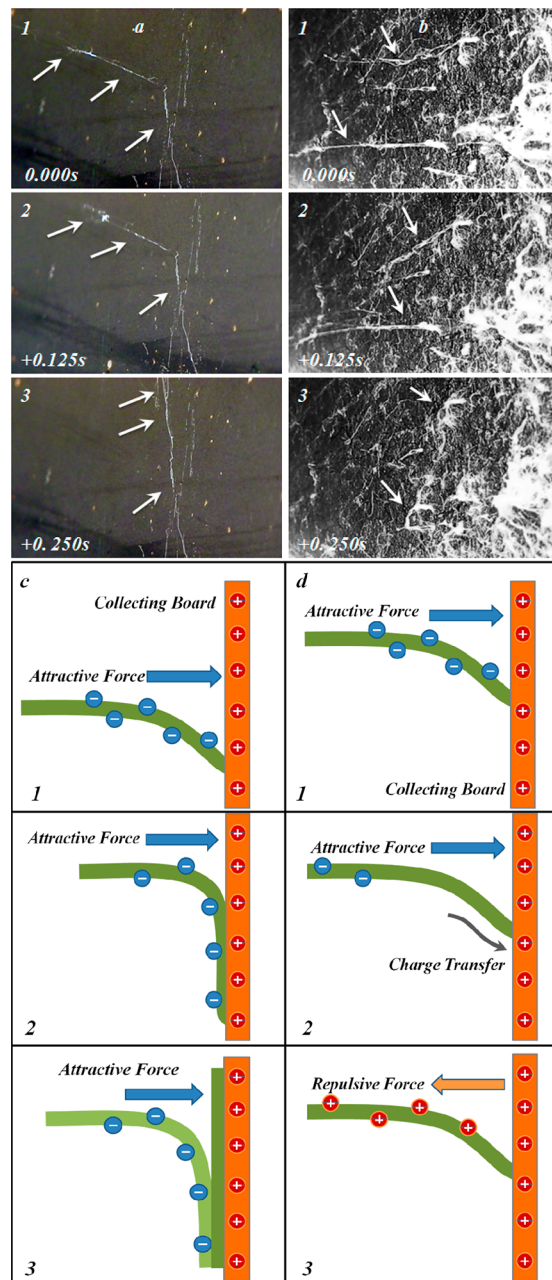


Figure 3. (a, b) Continuous photography of deposition processes of PEG fibers in 2D (a) electrospinning and 3D (b) electrospinning with time interval of 0.125 s between two sequential photographs. White objects in the images were PEG fibrous bulks. (c, d) Schematic diagram of deposition of fibers in 2D (c) and 3D (d) electrospinning processes. The needle was negatively charged, and the collecting board was positively charged. Orange, the collecting board; dark green, fibers deposited on the collecting board at the beginning; light green, fibers deposited on the collecting board afterward; blue arrow, attractive force; orange arrow, repulsive force; gray arrow, the direction of electron transfer; blue circle, negative charge; red circle, positive charge.

scaffolds and corresponding polymer surface resistivity. As shown in Figure 4a, the residual standard error of the model is 0.613, which is a reasonable number to indicate that the data could be well described by power function and suggest that there is a strong quantitative relationship between the specific

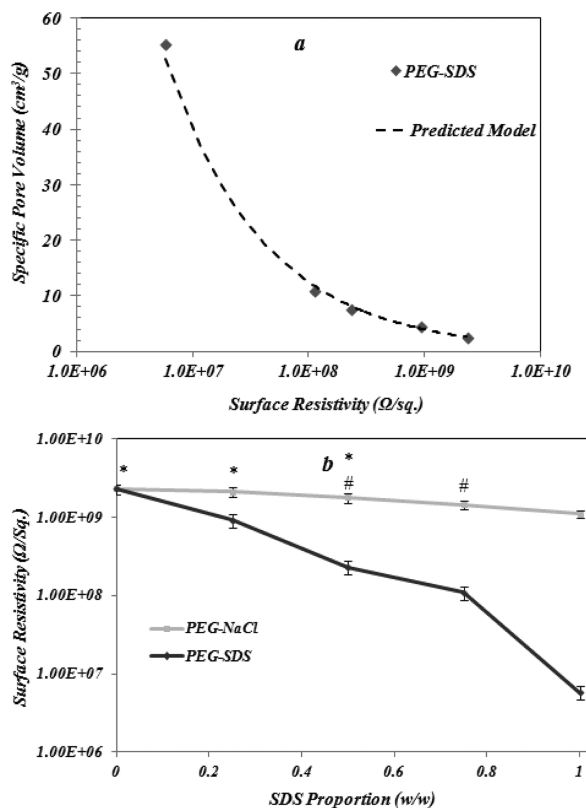


Figure 4. (a) Relationship between specific pore volume of electrospun scaffolds and surface resistivity. The dashed line shows the simulated relation using power function. (b) Effect of sodium dodecyl sulfate (SDS) and NaCl on surface resistivity of PEG films based on the proportions of SDS to polymer. The molar concentration of NaCl was the same as that of SDS at each point.

pore volume and surface resistivity. Hence, it verifies the theory proposed above. The power function was constructed as

$$y = ax^b \quad (1)$$

where y represented specific pore volume, x represented surface resistivity, and a and b were coefficients varied with the type of materials. Here, for PEG, a equaled to 2.208×10^5 and b equaled to -0.5325 . The specific pore volume decreased exponentially as surface resistivity increased. As surface resistivity decreased from 10^9 to $10^6 \Omega/\text{sq}$, the macrostructure of PEG scaffolds converted from 3D to 2D, and the specific pore volume decreased by about 20 times. It could be inferred that the increased surface conductivity increased fluffiness of scaffolds exponentially.

It was found that surface resistivity of the polymer decreased with increasing SDS proportion. As shown in Figure 4b, surface resistivity of PEG decreased as SDS content increased. Surface resistivity of pure PEG was higher than $10^9 \Omega/\text{sq}$. When the weight ratio of SDS to PEG was increased to 1:1, surface resistivity was reduced considerably to $10^6 \Omega/\text{sq}$. However, when NaCl was added into the polymer, the surface resistivity did not decrease as substantially as the same mole of SDS was added. This is because when water evaporated, SDS mainly distributed on the surface of polymer while NaCl may distribute more evenly in the polymer. The sulfate groups of SDS that concentrated on the surface of fiber oriented toward the outside,³⁵ and could induce formation of a surface water layer on the fibers. In the surface water layer of PEG fibers, free

movement of dissociable sodium ions from SDS effectively decreased surface resistivity of PEG electrospun fibers.³⁶ Whereas the evenly distributed NaCl would only decrease the volume resistivity but could not effectively decrease surface resistivity of fibers. In summary, by adding SDS, the polymer was converted from insulator to semiconductor,³⁶ the capability of transferring static electricity of the fiber has been tremendously increased, and this correspondingly increased the fluffiness of scaffolds.

To further investigate the effect of electron transference on formation of 3D architectures, a solution with 25 wt % zein and 25 wt % SDS was electrospun onto the positively charged collecting board covered by a layer of insulator. Delivery of electrons was interrupted though positive potential still existed. Zein fibers with electrons on the surface were attracted by the positive collector and then hit the board vertically as shown in Figure 5a. However, the electrons could not be transferred onto the collecting board and thus remained on the fibers. The highly negatively charged fibers attached onto the insulator tightly owing to the strong electrical attraction, and

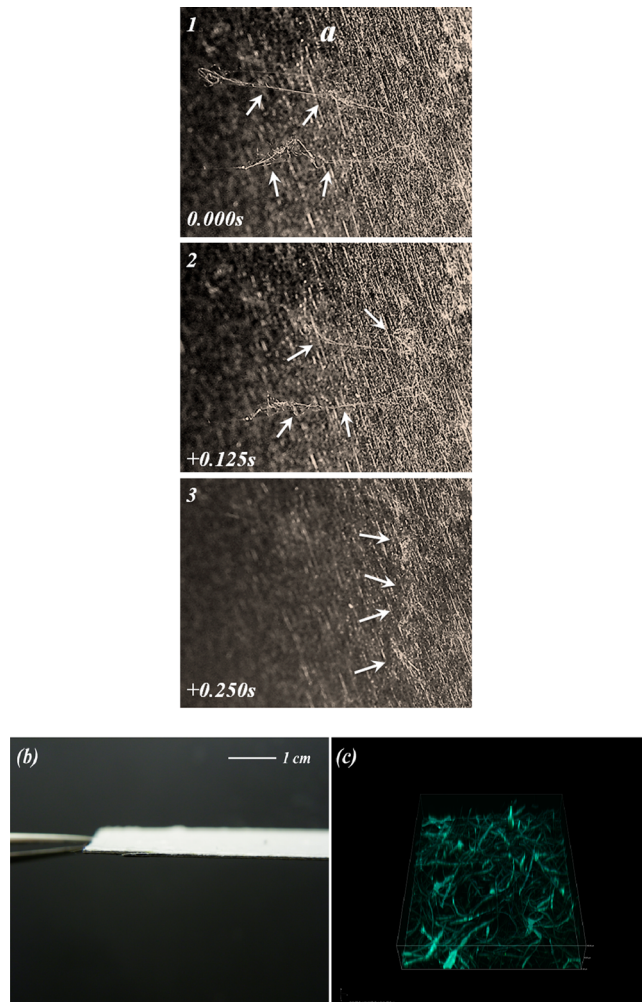


Figure 5. (a) Deposition process of zein onto the insulator covered collector with time interval of 0.125 s between two sequential photographs. The spinning dope consisted of 25 wt % zein and 25 wt % SDS. (b) Digital photo of the as-spun zein scaffold produced by electrospinning spinning dope with 25 wt % zein and 25 wt % SDS. (c) CLSM 45° view images at magnification of 100X of the above as-spun zein scaffold.

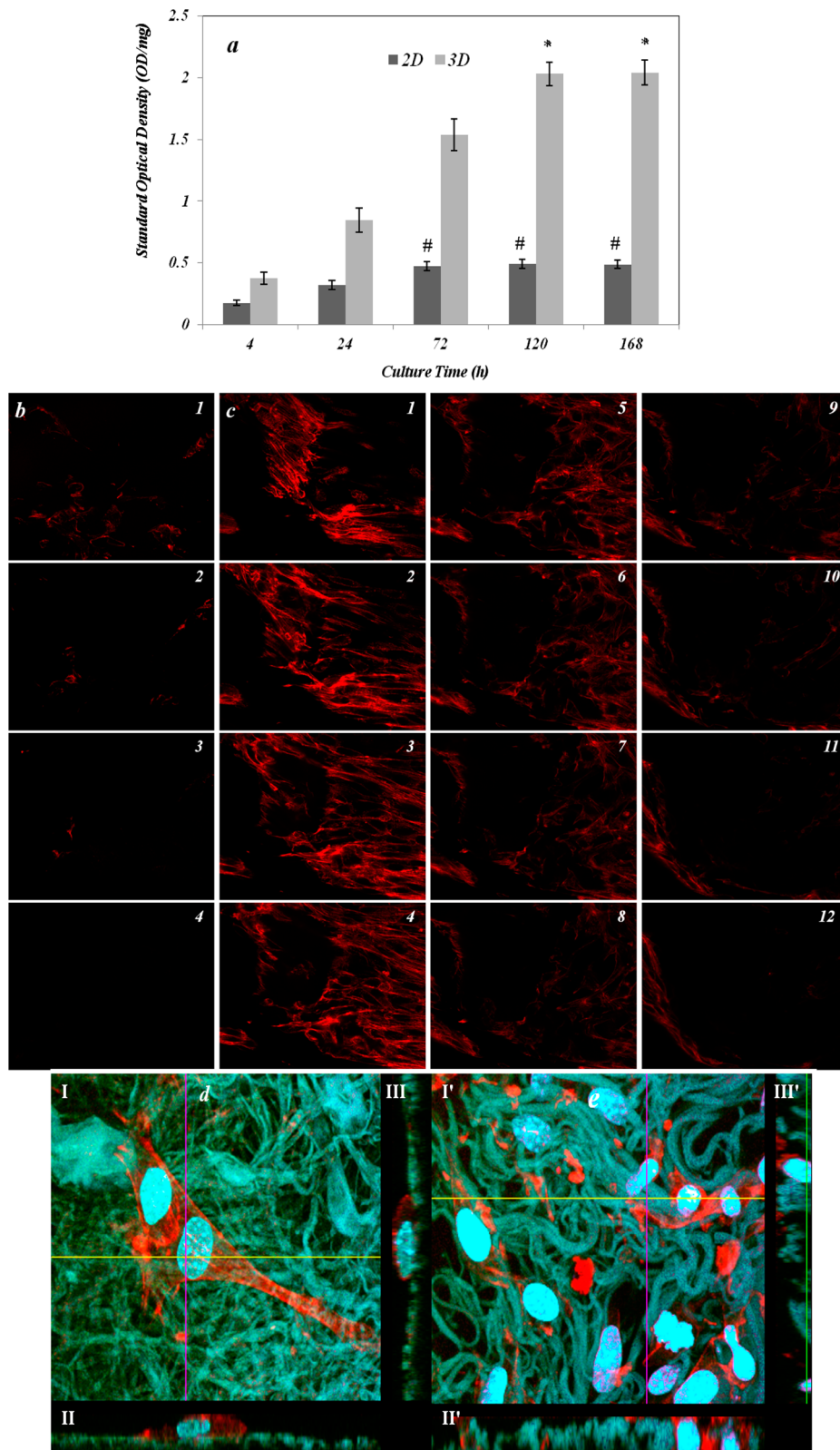


Figure 6. (a) MTS assay results of attachment (4 h) and proliferation (24, 72, 120, and 168 h) of NIH 3T3 fibroblast cells on 2D and 3D zein electrospun scaffolds. (b) 2D and (c) 3D zein electrospun scaffolds of CLSM montage images in sequential sections at 10 μm intervals under a magnification of 60 \times . The red network illustrates F-actin in NIH 3T3 cells stained with Phalloidin 633 at different depths from the surface after culture for 72 h. (d, e) CLSM images showing spreading of Phalloidin 633 and Hoechst 33342 stained NIH 3T3 cell on 2D and 3D zein electrospun scaffolds 48 h after seeding. Three dimensional reconstructions: xy projections (I and I'); xz projections (II and II'); and yz projections (III and III').

consequently a traditional 2D electrospinning scaffold (Figure 5b and c) was formed. As a conclusion, the proposed theory

that rapid delivery of electrons on the fibers was the crucial factor for formation of 3D architectures had high validity.

2.3. In Vitro Study. In vitro cell culture study results showed the 3D scaffolds were remarkably better than 2D scaffolds to support cell growth. As shown in Figure 6a, noteworthy increase in attachment and proliferation rates of fibroblast cells was found in 3D scaffolds. The amount of cells attached on 3D scaffolds was 114% higher than that on 2D scaffolds. A plateau of methanethiosulfonate (MTS) results was reached 5 days after cell cultured on 3D scaffolds and the proliferation of cells increased by 439%. For 2D scaffolds, the plateau of MTS result was found 3 days after seeding, and the proliferation of cells increased by 181%. Most currently reported 3D scaffolds only showed 1.5- to 2.5-fold improvement on comparison of 3D scaffolds with their 2D counterparts after 5–7 days of cell culture.^{37–39} The results were consistent with the observation in the CLSM montage images in Figure 6b and c. After 72 h of cell culture, cells were found at least 120 μm beneath the surface of the 3D scaffold, while cells could not be found 20–30 μm under the surface of the 2D scaffold. The tight packing of fibers in the 2D scaffolds restricted penetration of cells vertically, while the multiple pores with much larger size and significantly higher porosity of 3D scaffolds facilitated migration and penetration of cells into the interior of the structures.

What is more important, the spheroid-shaped three-dimensional cells on 3D scaffolds and flattened morphologies of cells on 2D scaffolds are shown in Figure 6d and e. In Figure 6d.I, the developed cytoskeletons of cells, which were indicated by the actin filaments stained in red, spread over the surface of 2D scaffold. As illustrated in xz projection in Figure 6d.II and yz projection in Figure 6d.III, thicknesses of the individual cells were much smaller than their planar sizes as shown in the xy projection. Cells seeded in the 2D scaffolds tended to grow into planar morphologies, which differed from that of cells *in vivo*. However, the side views of 3D scaffolds in Figure 6e.II' and III' revealed that the same cells oriented in z direction rather than in x and y directions, since the lengths of cell nuclei in z direction were longer than the diameters of them in the xy projection. This result suggested that 3D scaffolds facilitated cells to develop into stereoscopic topographies that more closely mimic the cells in many native ECMs. It is of great potential that 3D regenerated tissues with satisfactory physiological morphologies and functions could be fabricated by integration of proper cells into the 3D electrospun scaffolds.

3. CONCLUSIONS

In summary, novel 3D zein and PEG electrospun scaffolds with three-dimensionally and randomly oriented fibers and large interconnected pores were successfully fabricated by reducing surface resistivity of materials. The 3D scaffolds could better mimic naturally occurring 3D ECMs with spatially arranged and randomly oriented protein fibers. The morphologies of cells cultured in the 3D scaffolds could grow into stereoscopic morphologies that were more close to cells in the native ECMs. In addition, remarkably better attachment, proliferation, and penetration of cells were found in the 3D zein scaffolds compared with 2D scaffolds. A mechanism that increased in surface conductivity of material during electrospinning and could induce formation of 3D electrospun structures was proposed and validated. The novel 3D electrospinning method could be applied to a number of water insoluble proteins and many other water-soluble materials.

4. EXPERIMENTAL SECTION

4.1. Scaffold Preparation. As adapted from previous work,³⁰ 2D zein scaffolds were prepared by electrospinning 25 wt % zein (Freeman Industries LLC, Tuckahoe, NY) in 70% v/v aqueous ethanol (EMD Chemicals Inc., Gibbstown, NJ) solution. Three dimensional zein scaffolds were prepared by electrospinning aqueous solution containing 25 wt % zein and 25 wt % SDS. A concentration of 9 wt % (based on the weight of zein) citric acid (EMD Chemicals Inc., Gibbstown, NJ) was added into both 2D and 3D spinning dopes for cross-linking. Different solvent systems were utilized since zein could not be dissolved in water. The 2D PEG scaffold was prepared by electrospinning 10 wt % PEG (50 kDa, Sigma-Aldrich, St. Louis, MO) aqueous solution. The 3D PEG scaffold was prepared by electrospinning 10 wt % PEG and 10 wt % SDS in aqueous solution. All the electrospinning parameters, including the extrusion speed of 2 mL h⁻¹, voltage of 42 kV, and distance from the needle to the collecting board of 25 cm, were kept the same for all the samples. The needle was negatively charged, and the collecting board was positively charged.

4.2. Morphologies and Structures of Scaffolds. The 2D and 3D scaffolds were observed using a scanning electron microscope (S3000N, Hitachi Inc. Schaumburg, IL) and a Nikon A1 confocal laser scanning microscope (Nikon Inc., Melville, NY).

4.3. Specific Pore Volume. Specific pore volume indicating volume of pore in unit mass of scaffolds as shown in eq 2 was selected to evaluate fluffiness of the scaffolds.

$$V_{\text{sp}} = \frac{V_{\text{pore}}}{m_{\text{scaffold}}} = \frac{V_{\text{scaffold}}}{m_{\text{scaffold}}} - \frac{1}{\rho_{\text{material}}} \quad (2)$$

where V_{sp} is the specific pore volume, V_{pore} is the volume of pores encompassed in the scaffolds, m_{scaffold} is the mass of scaffolds, V_{scaffold} is the volume of the scaffolds after precise measurement of the length, width, and thickness of scaffolds, and ρ_{material} is the density of the material.

4.4. Surface Resistivity. Since the surface resistivity of ultrafine fibers is very difficult to test, films containing same polymer to surfactant/salt ratio with relevant electrospun fibers were prepared to measure the surface resistivity. The films were casted onto Teflon coated plates and dried at 20 °C and 65% relative humidity. Surface resistivity was measured by employing a surface resistivity tester (Monroe Electronics Inc., Lyndonville, NY) according to ASTM D-257 standard.

4.5. Fiber Deposition Process. A CCD camera with a long-working-distance lens was used in capturing the moment photographs of fiber deposition and scaffold formation. The time interval for each consequential photograph was 0.125 s.

4.6. Cell Attachment and Proliferation. NIH 3T3 mouse fibroblast cells (ATCC CRL-1658, Manassas, VA) were cultured to quantitatively estimate effects of 2D and 3D structures of zein scaffolds on cell attachment and proliferation. Cells were cultured in culture medium at 37 °C in a humidified 5% CO₂ atmosphere. Electrospun 2D and 3D zein scaffolds were first rinsed in 60 wt % acetone (BDH, West Chester, PA) aqueous solution containing 5 wt % potassium chloride (Fisher Scientific, Fair Lawn, NJ) to remove SDS, washed in distilled water three times, and then lyophilized. MTS assays were performed to quantitatively investigate cell viability at attachment and proliferation stages. Samples were prepared with same weight and then were subjected to sterilization at 120 °C for 1 h. After sterilization, the scaffolds were placed in 48-well culture plates (TPP Techno Plastic Products, Switzerland). Fibroblast cells were seeded onto the scaffolds (1 × 10³ cells mL⁻¹, 500 μL well⁻¹) and then cultured at 37 °C in a humidified 5% CO₂ atmosphere for different time intervals. At each time point, the samples were washed with PBS, placed in new 48-well plates containing 450 μL well⁻¹ 20% MTS reagent (CellTiter 96 Aqueous One Solution Cell Proliferation Assay, Promenade) in Dulbecco's modified Eagle's medium (DMEM) and incubated at 37 °C in a humidified 5% CO₂ atmosphere for 3 h. After incubation, 150 μL of the solution from each well was pipetted into a 96-well plate and the optical densities were measured at 490 nm using a UV-vis

multiplate spectrophotometer (Multiskan Spectrum, Thermo Scientific). The MTS solution in DMEM without cells served as the blank.

4.7. Cell Penetration and Spreading. To compare penetration ability of cells on 2D and 3D scaffolds, cells were stained by Phalloidin 633 solution (1:200 Alexa Fluor 633 Phalloidin, Invitrogen, Grand Island, NY) and observed using a Nikon A1 confocal laser scanning microscope (Nikon Inc., Melville, NY). Alexa Fluor 633 Phalloidin is a far red fluorescent dye that specifically bonds to F-actin in cells. This dye was selected since zein shows fluorescence across the full spectrum with weakest signal in the far red range. To observe the spreading behaviors and stereoscopic morphologies of cells in 2D and 3D scaffolds, cells were stained by Phalloidin 633 solution for F-actin and Hoechst 33342 solution (Invitrogen, Grand Island, NY) for the nuclei of cells.

4.8. Statistical Analysis. One-way analysis of variance with Tukey's pairwise multiple comparisons was employed to analyze the data. The confidence interval was set at 95%, and a *P* value less than 0.05 was considered to be a statistically significant difference. In the results, data labeled with different symbols were significantly different from each other.

AUTHOR INFORMATION

Corresponding Author

*E-mail: yyang2@unl.edu.

Author Contributions

The manuscript was written through contributions of all authors. All authors have given approval to the final version of the manuscript.

Notes

The authors declare no competing financial interest.

ACKNOWLEDGMENTS

The authors thank the awards of John and Louise Skala Fellowship for Shaobo Cai and Helan Xu. The authors also would like to acknowledge Teresa Fangman, Christian Elowsky, and Dr. You Zhou for their help in the CLSM experiments and Fan Yang for her assistance in the statistical analysis. This research was financially supported by the Nebraska Corn Board, Agricultural Research Division at the University of Nebraska—Lincoln, USDA Hatch Act, Multistate Research Project S-1054 (NEB37-037).

REFERENCES

- (1) Shastri, V. P. In vivo Engineering of Tissues: Biological Considerations, Challenges, Strategies, and Future Directions. *Adv. Mater.* **2009**, *21*, 3246–3254.
- (2) Bhattarai, N.; Li, Z. S.; Edmondson, D.; Zhang, M. Q. Alginate-based nanofibrous scaffolds: Structural, mechanical, and biological properties. *Adv. Mater.* **2006**, *18*, 1463–1467.
- (3) Dvir, T.; Timko, B. P.; Kohane, D. S.; Langer, R. Nanotechnological strategies for engineering complex tissues. *Nat. Nanotechnol.* **2011**, *6*, 13–22.
- (4) Roskelley, C. D.; Desprez, P. Y.; Bissell, M. J. Extracellular Matrix-Dependent Tissue-Specific Gene-Expression in Mammary Epithelial-Cells Requires Both Physical and Biochemical Signal-Transduction. *Proc. Natl. Acad. Sci. U.S.A.* **1994**, *91*, 12378–12382.
- (5) Yamada, K. M.; Cukierman, E. Modeling tissue morphogenesis and cancer in 3D. *Cell* **2007**, *130*, 601–610.
- (6) Smalley, K. S. M.; Lioni, M.; Herlyn, M. Life isn't flat: Taking cancer biology to the next dimension. *In Vitro Cell. Dev. Biol.: Anim.* **2006**, *42*, 242–247.
- (7) Bosman, F. T.; Stamenkovic, I. Functional structure and composition of the extracellular matrix. *J. Pathol.* **2003**, *200*, 423–428.
- (8) Bissell, M. J.; Rizki, A.; Mian, I. S. Tissue architecture: the ultimate regulator of breast epithelial function - Commentary. *Curr. Opin. Cell. Biol.* **2003**, *15*, 753–762.
- (9) Uygun, B. E.; Soto-Gutierrez, A.; Yagi, H.; Izamis, M. L.; Guzzardi, M. A.; Shulman, C.; Milwid, J.; Kobayashi, N.; Tilles, A.; Berthiaume, F.; Hertl, M.; Nahmias, Y.; Yarmush, M. L.; Uygun, K. Organ reengineering through development of a transplantable recellularized liver graft using decellularized liver matrix. *Nat. Med.* **2010**, *16*, 814–820.
- (10) Zegers, M. M. P.; O'Brien, L. E.; Yu, W.; Datta, A.; Mostov, K. E. Epithelial polarity and tubulogenesis in vitro. *Trends Cell Biol.* **2003**, *13*, 169–176.
- (11) Petersen, T. H.; Calle, E. A.; Zhao, L. P.; Lee, E. J.; Gui, L. Q.; Raredon, M. B.; Gavrilov, K.; Yi, T.; Zhuang, Z. W.; Breuer, C.; Herzog, E.; Niklason, L. E. Tissue-Engineered Lungs for in Vivo Implantation. *Science* **2010**, *329*, 538–541.
- (12) Zhu, J.; Li, J.; Wang, B.; Zhang, W. J.; Zhou, G. D.; Cao, Y. L.; Liu, W. The regulation of phenotype of cultured tenocytes by microgrooved surface structure. *Biomaterials* **2010**, *31*, 6952–6958.
- (13) Cukierman, E.; Pankov, R.; Yamada, K. M. Cell interactions with three-dimensional matrices. *Curr. Opin. Cell. Biol.* **2002**, *14*, 633–639.
- (14) Griffith, L. G.; Swartz, M. Capturing complex 3D tissue physiology in vitro. *A. Nat. Rev. Mol. Cell. Biol.* **2006**, *7*, 211–224.
- (15) Lu, H. H.; Subramony, S. D.; Boushell, M. K.; Zhang, X. Z. Tissue Engineering Strategies for the Regeneration of Orthopedic Interfaces. *Ann. Biomed. Eng.* **2010**, *38*, 2142–2154.
- (16) Mikos, A. G.; Herring, S. W.; Ochareon, P.; Elisseeff, J.; Lu, H. H.; Kandel, R.; Schoen, F. J.; Toner, M.; Mooney, D.; Atala, A.; Van Dyke, M. E.; Kaplan, D.; Vunjak-Novakovic, G. Engineering complex tissues. *Tissue Eng.* **2006**, *12*, 3307–3339.
- (17) Saha, S.; Duan, X.; Wu, L.; Lo, P. K.; Chen, H.; Wang, Q. Electrospun fibrous scaffolds promote breast cancer cell alignment and epithelial-mesenchymal transition. *Langmuir* **2012**, *28*, 2028–34.
- (18) Haycock, J. W. 3D Cell Culture: A Review of Current Approaches and Techniques. *Methods Mol. Biol.* **2011**, *695*, 1–15.
- (19) Luo, Y.; Wang, S. G.; Shen, M. W.; Qi, R. L.; Fang, Y.; Guo, R.; Cai, H. D.; Cao, X. Y.; Tomas, H.; Zhu, M. F.; Shi, X. Y. Carbon nanotube-incorporated multilayered cellulose acetate nanofibers for tissue engineering applications. *Carbohydr. Polym.* **2013**, *91*, 419–427.
- (20) Li, D.; Xia, Y. N. Electrospinning of nanofibers: Reinventing the wheel? *Adv. Mater.* **2004**, *16*, 1151–1170.
- (21) Wang, S. G.; Castro, R.; An, X.; Song, C. L.; Luo, Y.; Shen, M. W.; Tomas, H.; Shi, X. Y. Electrospun laponite-doped poly(lactic-co-glycolic acid) nanofiber for osteogenic differentiation of human mesenchymal stem cells. *J. Mater. Chem.* **2012**, *22*, 23357–23367.
- (22) Liao, H. H.; Qi, R. L.; Shen, M. W.; Cao, X. Y.; Guo, R.; Zhang, Y. Z.; Shi, X. Y. Improved cellular response on multiwalled carbon nanotube-incorporated electrospun polyvinyl alcohol/chitosan nanofibrous scaffolds. *Colloids Surf., B* **2011**, *84*, 528–535.
- (23) Pham, Q. P.; Sharma, U.; Mikos, A. G. Electrospinning of polymeric nanofibers for tissue engineering applications: A review. *Tissue. Eng.* **2006**, *12*, 1197–1211.
- (24) Nandakumar, A.; Yang, L.; Habibovic, P.; van Blitterswijk, C. Calcium phosphate coated electrospun fiber matrices as scaffolds for bone tissue engineering. *Langmuir* **2010**, *26*, 7380–7.
- (25) Debnath, J.; Brugge, J. S. Modelling glandular epithelial cancers in three-dimensional cultures. *Nat. Rev. Cancer* **2005**, *5*, 675–688.
- (26) Hu, J.; Liu, X. H.; Ma, P. X. Induction of osteoblast differentiation phenotype on poly(L-lactic acid) nanofibrous matrix. *Biomaterials* **2008**, *29*, 3815–3821.
- (27) Moroni, L.; Schoteler, R.; Hamann, D.; de Wijn, J. R.; van Blitterswijk, C. A. 3D fiber-deposited electrospun integrated scaffolds enhance cartilage tissue formation. *Adv. Funct. Mater.* **2008**, *18*, 53–60.
- (28) Yokoyama, Y.; Hattori, S.; Yoshikawa, C.; Yasuda, Y.; Koyama, H.; Takato, T.; Kobayashi, H. Novel wet electrospinning system for fabrication of spongiform nanofiber 3-dimensional fabric. *Mater. Lett.* **2009**, *63*, 754–756.
- (29) Simonet, M.; Schneider, O. D.; Neuenschwander, P.; Stark, W. J. Ultraporous 3D polymer meshes by low-temperature electrospinning: Use of ice crystals as a removable void template. *Polym. Eng. Sci.* **2007**, *47*, 2020–2026.

- (30) Bonino, C. A.; Efimenko, K.; Jeong, S. I.; Krebs, M. D.; Alsberg, E.; Khan, S. A. Three-Dimensional Electrospun Alginate Nanofiber Mats via Tailored Charge Repulsions. *Small* **2012**, *8*, 1928–1936.
- (31) Jiang, Q. R.; Reddy, N.; Yang, Y. Q. Cytocompatible cross-linking of electrospun zein fibers for the development of water-stable tissue engineering scaffolds. *Acta Biomater.* **2010**, *6*, 4042–4051.
- (32) Ma, P. X. Biomimetic materials for tissue engineering. *Adv. Drug Delivery Rev.* **2008**, *60*, 184–198.
- (33) Birgersdotter, A.; Sandberg, R.; Ernberg, I. Gene expression perturbation in vitro - A growing case for three-dimensional (3D) culture systems. *Semin. Cancer Biol.* **2005**, *15*, 405–412.
- (34) Drury, J. L.; Mooney, D. J. Hydrogels for tissue engineering: scaffold design variables and applications. *Biomaterials* **2003**, *24*, 4337–4351.
- (35) Fainerman, V. B.; Möbius, D.; Miller, R. *Surfactants: chemistry, interfacial properties, applications*, 1st ed.; Elsevier Science, Ltd.: Amsterdam; New York, 2001; pp 20–43.
- (36) Ranney, M. W. *Antistatic agents: technology and applications*, 1972; Noyes Data Corp.: Park Ridge, NJ, 1972; pp 113–162.
- (37) Cai, Y. Z.; Zhang, G. R.; Wang, L. L.; Jiang, Y. Z.; Ouyang, H. W.; Zou, X. H. Novel biodegradable three-dimensional macroporous scaffold using aligned electrospun nanofibrous yarns for bone tissue engineering. *J. Biomed. Mater. Res., Part A* **2012**, *100A*, 1187–1194.
- (38) Hosseinkhani, H.; Hosseinkhani, M.; Hattori, S.; Matsuoka, R.; Kawaguchi, N. Micro and nano-scale in vitro 3D culture system for cardiac stem cells. *J. Biomed. Mater. Res., Part A* **2010**, *94A*, 1–8.
- (39) Zhu, X. L.; Cui, W. G.; Li, X. H.; Jin, Y. Electrospun fibrous mats with high porosity as potential scaffolds for skin tissue engineering. *Biomacromolecules* **2008**, *9*, 1795–1801.